

## The Variation of Mechanical Properties of M300 Maraging Steel Manufactured with Varying Process Parameters in Laser Powder Bed Fusion

Haley E. Petersen<sup>1,2</sup>, Brad J. Sampson<sup>1,2</sup>, David P. Failla Jr.<sup>1,2</sup>, Matthew W. Priddy<sup>1,2</sup>, and Zackery B. McClelland<sup>3</sup>

<sup>1</sup>Department of Mechanical Engineering, Mississippi State University, Mississippi State, MS, 39762

<sup>2</sup>Center of Advanced Vehicular Systems, Starkville, MS, 39759

<sup>3</sup>US Army Engineer Research and Development Center, Vicksburg, MS 39180

### Abstract

Laser powder bed fusion (L-PBF) is a type of additive manufacturing (AM) that uses layers of powdered metal and a laser to manufacture a part in a layer-by-layer fashion. L-PBF uses a variety of process parameters that ultimately determine the overall quality and mechanical properties of a print. The ability to alter parameters allows for the utilization of various metals in this form of AM. Maraging 300 steel (M300) is a material of particular interest due to its combined tensile strength and high strength-to-weight ratio. By using an assortment of parameters and comparing the resulting mechanical properties it can be determined which process parameters result in a more favorable part to be used in a variety of applications. A favorable process parameter set was selected for future use. This study aims to determine which process parameters result in the best overall mechanical properties of M300 manufactured using L-PBF.

### Introduction

Additive manufacturing (AM) is a manufacturing technique that has been around for more than 20 years when it was originally introduced, the main application was for rapid prototyping. Initially, the porosity of the parts was not an issue due to the intended use of the developed parts. As technology advances more applications have developed and with that the ability to create more complex and dense parts. There are various types of AM and can be performed with various mediums, generally, each medium requires a different machine type. One of the materials that is of interest to various industries is metal. With a variety of types of metal AM a variety of properties can be achieved. An AM technique that results in unique properties and microstructure is laser powder bed fusion (L-PBF). This process systematically uses fine layers of metal powder and a high-power laser to fuse the metal and build a solid part. This layer-by-layer process produces a uniquely fine microstructure as well as allows for geometric freedom that cannot be achieved with traditional manufacturing.

Maraging Steel is a high-strength martensitic steel that is commonly used in a large scope of applications in industries like aerospace/marine, defense, and industrial [1]. This steel is not only favorable due to its high strength but also its weldability and ease of heat treatment. There are four different strengths of maraging steel (200, 250, 300, 350) these strength ranges allow a tailored coverage of strength and toughness [1]. This investigation is centered around strength grade 300, often referred to as M300, the chemical composition of M300 is shown in Table 1.

**Table 1:** Chemical composition of Maraging 300 Steel (M300) powder (wt%) [2]

Ni	Mo	Co	Ti	Al	Cr	Cu	Mn	Si	Fe
17.25 ± 0.45	4.57 ± 0.08	9.11 ± 0.23	0.84 ± 0.18	0.89 ± 0.10	0.10 ± 0.07	0.09 ± 0.05	0.04 ± 0.03	0.04 ± 0.02	Bal.

The strengthening characteristics of M300 come due to the lack of carbon, allowing for second-phase precipitates to form instead of carbide precipitates. These compounds form a fine distribution throughout the softer Fe-Ni matrix which allows conditions of strengthening to occur [1]. Wrought M300 is high strength and high toughness steel, which generally has mechanical properties as follows; yield 1790-2070 MPa, ultimate tensile strength (UTS) 1830-2100 MPa, young's modulus 183-193 GPa, and elongation at break of 5-10% [3].

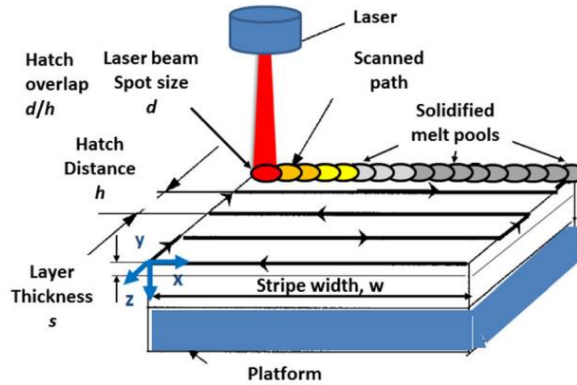


**Figure 1:** Schematic of several process parameters of the Laser Powder Bed Fusion (L-PBF) [4]

Parts manufactured using M300 are used for various reasons, this process results in a fine microstructure and the ability to customize mechanical properties by altering process parameters. Process parameters are settings that determine the method in which a part is manufactured. Ultimately these settings affect the amount of heat that is input into the sample. Process parameters include laser power, spot diameter, scan speed, point/hatch distance, scan strategy, and layer thickness; a schematic of process parameters used in L-PBF is shown in **Figure 1**. These properties influence the overall quality of print as well as the microstructure, density, porosity, defects, and residual stress. Evaluating the effect that each parameter has on a print can be a challenge due to the large number of parameters, printers, and material. However, one way to evaluate a set of parameters against each other is the energy density. The energy density (E) is a value that is a result of several parameters, energy density is a function of laser power (P), scan speed (v), hatch distance (h), and layer height (t) and is calculated using the equation **Error! Not a valid bookmark self-reference.** [5]. Energy density calculates the amount of energy that is input into the sample. The printing objective is to have an energy that is large enough for all powder to completely melt, epitaxial solidification, and form a fully dense part [6].

$$E = \frac{P}{(v \times h \times t)} \quad 1$$

Literature investigates a large number of variables, print parameters, printers, and any mechanical properties. This information was compiled and used for comparison, allowing evaluation of the process-properties-performance relationship. A compilation of data is shown in

**Figure 2.** In these figures, size, and color of the points is a representation of the energy density versus the recorded mechanical property. From this data a general conclusion can be made regarding the energy density, relative density, and hardness of the material. As the energy density increases the relative density and the hardness of the material increases (**Figure 2**). As shown in the figure below there is not a distinguishable trend between the energy density, relative density, and the other recorded mechanical properties. The process-property-performance relationship presents a challenge in developing a set of ideal parameters set to print M300 parts. In addition, the overall lack of a trend also makes the prediction of a sample properties given energy density difficult.

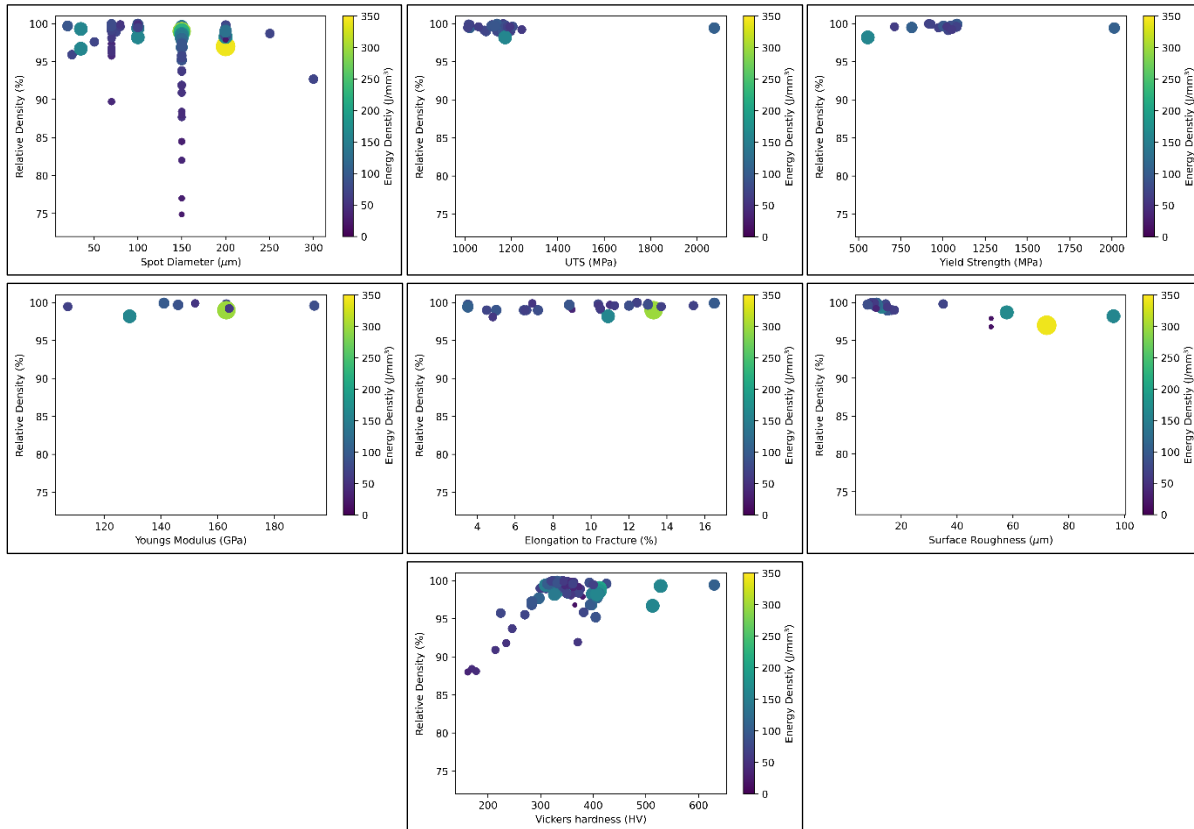


**Figure 2:** Maraging 300 Steel manufactured using L-PBF with varying parameters Mechanical Properties vs. Relative Density vs. Energy Density [2], [3], [5]–[12], [13, p. 18], [14]–[24], [24], [25], [25]–[48]

Other considerations to consider in parameter sets analysis is location and orientation on the build plate. These variables have been found to affect the part’s performance as well as the overall quality of the print [27], [49].

The current study aims to determine the ideal process parameters that result in the most favorable mechanical properties when printing M300 on a Renishaw AM400. Process parameters including laser power and scan speed are varied. Specimens are then analyzed utilizing mechanical characterization techniques such as tension tests, microhardness indentation, and surface

roughness. The data is then collected, compiled and analyzed will allow for the determination of the most favorable properties.

## Methods

### Selection of process parameters

In this study, all prints are performed on a Renishaw AM400 using Gas-atomized M300 maraging steel powder supplied by Carpenter Additive with a chemical composition shown in **Error! Not a valid bookmark self-reference.** For a starting point, the process parameters that Renishaw provided are use, this is denoted as parameter set 1 in **Table 3** were used. The energy density of the given parameter set (Set 1) was calculated and nine other process parameters were calculated using a range of energy densities shown in **Table 3**. These ten parameter sets, shown in Table 3, are the sets studied in this investigation.

*Table 2: Chemical composition of Carpenter Additive produced gas atomized M300 maraging steel powder [50]*

Element	Ni	Co	Mo	Ti	Cr	Fe
Composition (%)	17-19	8.5-10	4.5-5.2	0.8-1.12	0.25	Bal.

*Table 3: M300 maraging steel process parameter sets*

Parameter Set	Laser Power (W)	Scan Speed (mm/sec)	Spot Diameter (μm)	Hatch Distance (μm)	Layer Thickness (μm)	Exposure Time (μs)	Energy Density (J/mm <sup>3</sup> )
1	400	1000	70	95	40	60	<b>105.26</b>
2	400	700	70	95	40	85.7	<b>150.38</b>
3	400	1200	70	95	40	50	<b>87.72</b>
4	350	1000	70	95	40	60	<b>92.11</b>
5	350	700	70	95	40	85.7	<b>131.58</b>
6	300	700	70	95	40	85.7	<b>112.78</b>
7	300	1000	70	95	40	60	<b>78.95</b>
8	300	1200	70	95	40	50	<b>65.79</b>
9	250	700	70	95	40	85.7	<b>93.98</b>
10	250	1000	70	95	40	60	<b>65.79</b>

The geometry printed in this study was ATSM E8 rectangular 6 mm tensile specimens [51]. To account for the effect location each specimen was randomly placed on the build plate shown in **Figure 3**. This should allow the average properties to represent the overall properties of each set of six specimens. As shown in Figure 3 each specimen was labeled with the number of the parameter set it was assigned, its specimen number in that set, and a bracket (J), which denotes the corner that was facing the front of the plate. After the print was completed and the tensile specimens were removed from the build plate and the supports were removed from the specimen.

All specimens were then put into beakers and then into an ultrasonic cleaner with 99% isopropyl alcohol (IPA) for about 15 minutes to remove any loose powder on the part.

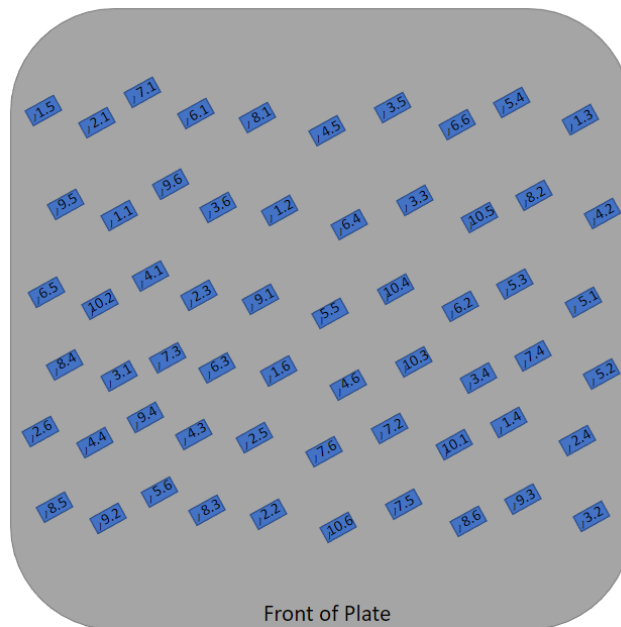


**Figure 3:** M300 maraging steel tensile specimen build plates (X.Y: X is the parameter set Y is the sample number)

### Mechanical Testing Procedure

Several mechanical tests were performed in this study including surface roughness, Vickers hardness, and tensile tests. Surface roughness measurements were performed on both sides of the width of the specimens using a Keyence VR-5000 optical profilometer. These measurements were taken to account for the parameters set effect on surface roughness. The parts orientation on the build plate was recorded and tracked which then tracked the difference between the side that comes in contact with the wiper and the roughness of the gas-facing side. Five-line measurements were taken on each side of the specimen, each side of the specimen's roughness is an average of those five measurements. Then, tension tests were performed on five of the specimens. These tests were performed using an Instron 5985 and an Instron video extensometer was used to track the reaction on the sample. Displacement-controlled tests were performed at 0.03 mm/s. Microhardness tests were then performed using a Struers DuraScan 70. Vickers hardness measurements were measured from the sixth specimen of each parameter set and from a chosen specimen. These measurements produced a median stress-strain curve during testing in both the build direction and perpendicular to the build direction. The sixth specimen was tested in the gauge section and the tested specimen was tested from the grip section to keep any strain hardening from affecting the resulting hardness values.

### Results and Discussion

The average surface roughness of each process parameter with a secondary axis of energy density is presented in **Error! Not a valid bookmark self-reference..** Based on the results of

Figure 4, the energy density is an indication of the surface roughness, in this study as the energy density increases the surface roughness increases.

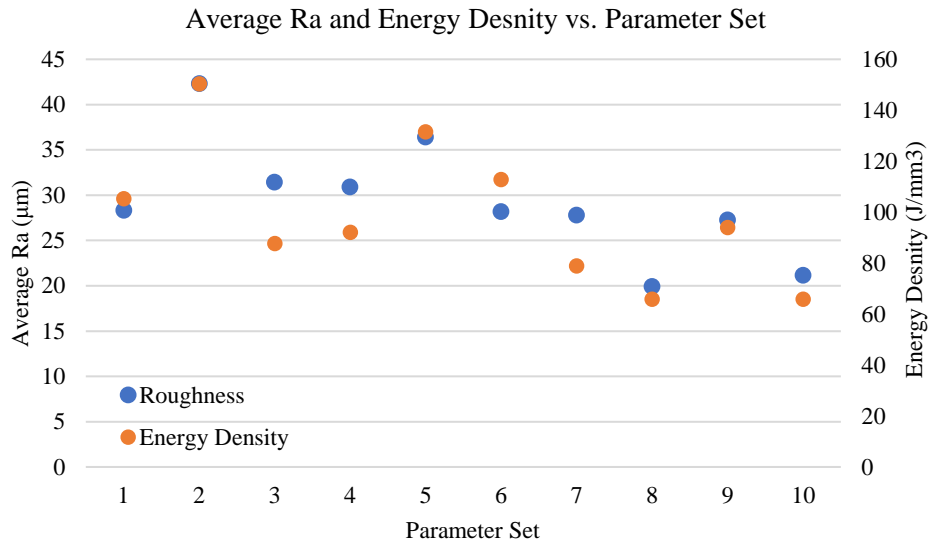


**Figure 4:** Average surface roughness of each process parameter set

Tension tests resulted in a variety of data seen in Figure 5. One specimen was chosen from each parameter set to represent the reaction of the parameter set. Based on the large spread of data, the variation of energy density is further confirmed to have a significant effect on the overall performance of the part. The average mechanical properties calculated from tension testing are presented in **Error! Not a valid bookmark self-reference..** Several of the parameters displayed a more brittle response than other parameters. From this evaluation, any specimen that presented an average percent elongation below 14% is considered too brittle and was excluded in the final selection of parameters. The strain hardening and necking regions fluctuate significantly between each parameter set, even within parameter sets there is fluctuation in those regions. Based on the results of **Error! Not a valid bookmark self-reference..**, if the energy density is less than 90 J/mm<sup>3</sup> this results in a more brittle mechanical response, which can be observed by the energy absorption seen in the curves in Figure 5.

**Table 4:** Average tensile properties of each parameter set

	P1	P2	P3	P4	P5	P6	P7	P8	P9	P10
Modulus of Elasticity (GPa)	82.15	73.57	108.58	108.59	80.84	90.64	108.06	117.91	105.67	110.31
Ultimate Tensile Strength (MPa)	1004.56	951.93	994.00	1005.30	965.44	1033.58	975.07	735.26	1020.31	1005.486
0.2% Yield Strength (MPa)	896.2	880.0	854.6	840.0	824.6	896.6	892.0	800.4	882.4	912.8
Percent Elongation (%)	16.65	18.47	12.39	15.83	17.17	18.63	11.53	7.88	15.44	11.02
Energy Density (J/mm <sup>3</sup> )	105.26	150.38	87.72	92.11	131.58	112.78	78.95	65.79	93.98	65.79
Energy Absorption	107.43	97.32	19.06	74.45	85.31	126.24	28.74	28.74	65.90	21.79

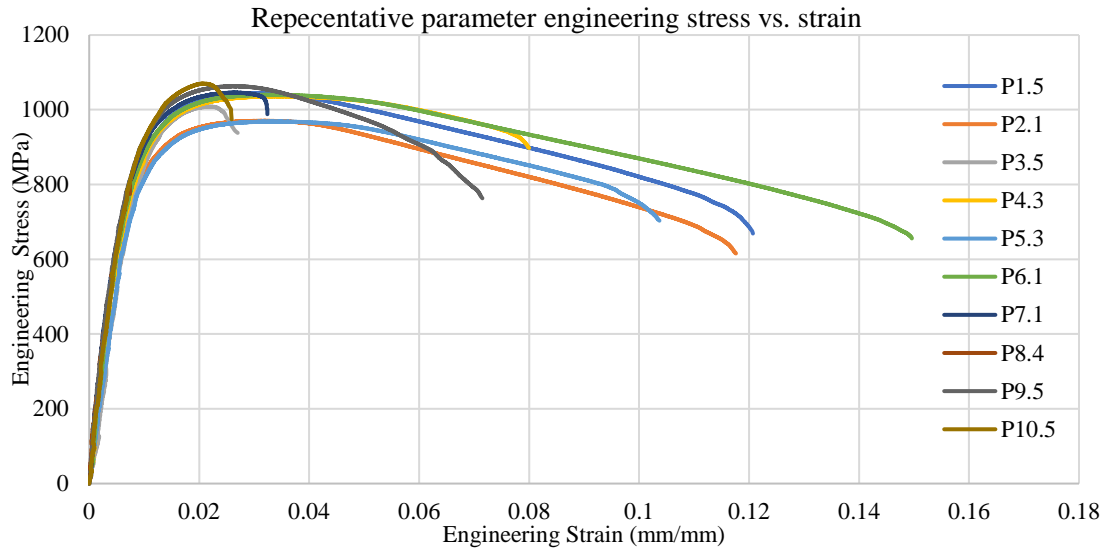


**Figure 5:** Engineering Stress vs. Engineering Strain of the median specimen in each parameter set

In **Figure 6:** Vickers hardness in build direction (BD) and perpendicular to the build direction (PBD) Figure 6, the Vickers hardness of the sixth and the selected median specimen collected from both the build and perpendicular to the build direction is shown. The plots have a large spread of values. Variation between the build and perpendicular build direction is expected due to the inherent anisotropy of L-PBF. The spread of hardness values is likely due to both the location on the build plate and the microstructure formation as the layers cool. Further work such as Electron Backscatter Diffraction (EBSD) and porosity analysis could help investigate the true cause of the spread of data.

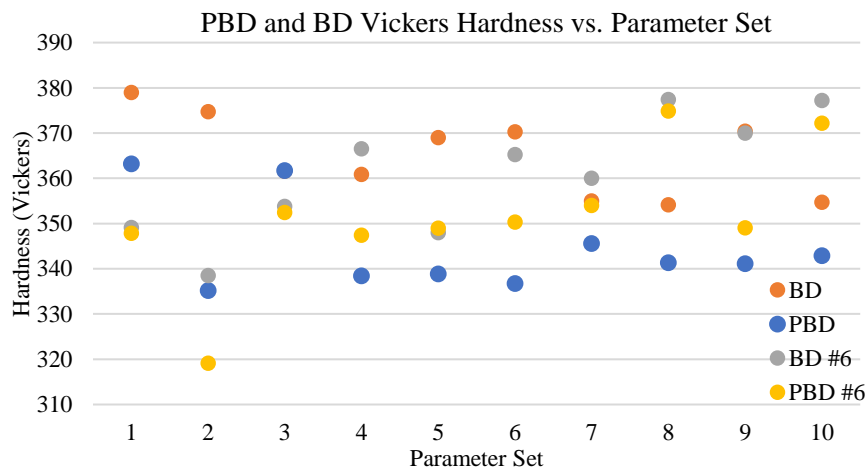


**Figure 6:** Vickers hardness in build direction (BD) and perpendicular to the build direction (PBD)

Based on the results presented, the overall energy density has a significant effect on the overall print quality and mechanical properties. Investigating the tensile test data (Figure 5,

Tension tests resulted in a variety of data seen in Figure 5. One specimen was chosen from each parameter set to represent the reaction of the parameter set. Based on the large spread of data, the variation of energy density is further confirmed to have a significant effect on the overall performance of the part. The average mechanical properties calculated from tension testing are presented in *Error! Not a valid bookmark self-reference.*. Several of the parameters displayed a more brittle response than other parameters. From this evaluation, any specimen that presented an average percent elongation below 14% is considered too brittle and was excluded in the final selection of parameters. The strain hardening and necking regions fluctuate significantly between each parameter set, even within parameter sets there is fluctuation in those regions. Based on the results of *Error! Not a valid bookmark self-reference.*, if the energy density is less than 90 J/mm<sup>3</sup> this results in a more brittle mechanical response, which can be observed by the energy absorption seen in the curves in Figure 5.

**Table 4)** several parameter sets can be discounted as possible ideal parameters. An energy density of less than 90 J/mm<sup>3</sup> resulted in a more brittle mechanical response. In this study it was observed that specimens that have energy density of 90 J/mm<sup>3</sup> produced a much smaller energy absorption compared to greater energy densities. This determination resulted in parameter set 3, 7, 8, and 10 being excluded from further consideration. In literature energy densities of less than 90 J/mm<sup>3</sup> result in a large range of reactions which is not consistent to the results observed in this study [5]–[12], [12], [22], [24], [25], [28], [30]–[32], [35], [36], [38], [41], [44], [46], [52]–[55]. In Figure 7Figure 8 the combination of data collected in this study and data from literature. Circled in red the orange points and green points are the points that were collected in this study, that shows the range of resulting properties. This could be due to the variation in printers, powder suppliers, and experimental methods used in literature. Additionally, parameter sets with higher energy densities, parameter sets 2 and 5, have lower energy absorbed during tensile testing. A further look into other data collected, yielded a conclusion that the set that absorbed the most energy seen in Figure 5 is parameter sets 1 and 6. Parameter set 6 has more consistent stress stain curves than parameter set 1. The green point in Figure 7Figure 8 represents parameter 6, this parameter set was selected due to the ductility, strength and energy absorption compared to the other parameter sets. Set 6 was found to have mechanical properties of; modulus of elasticity of 90.64 GPa, UTS of 1033.58 MPa, yield strength of 896.6 MPa, elongation of 18.63%. Combined with the hardness and surface roughness data parameter set 6 is selected as the most ideal parameter set.

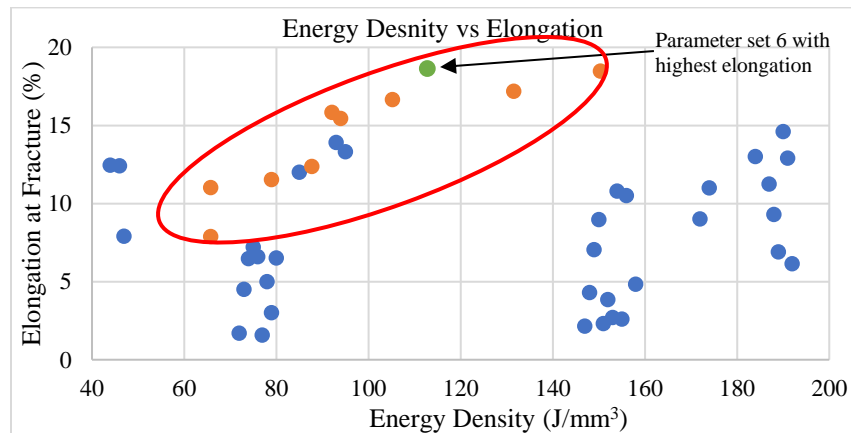


**Figure 7:** Energy Density vs. Elongation to fracture (blue points from literature, orange points is tested data, green points is selected parameter set 6) [2], [3], [5]–[12], [13, p. 18], [14]–[24], [24], [25], [25]–[48]

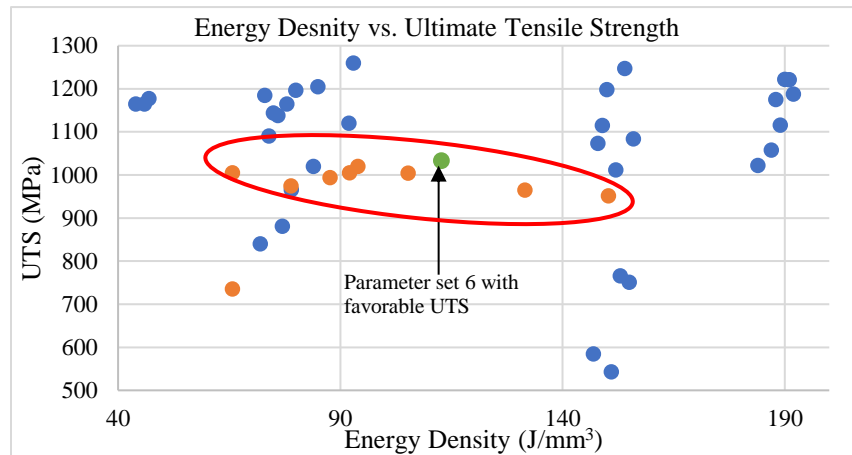


**Figure 8:** Energy Density vs. Ultimate Tensile Strength (Blue points from literature, orange points is tested data, green points is selected parameter set 6) [2], [3], [5]–[12], [13, p. 18], [14]–[24], [24], [25], [25]–[48]

### Conclusion

In this work, the effect of energy density input into a part and the resulting mechanical properties of M300 maraging steel parts produced using L-PBF were investigated. To change the energy density the laser power was varied from 400-250 W and scan speed was varied from 700-1200 mm/sec. The mechanical response was recorded between the energy density and the printed parts. Using the acquired mechanical response a parameter set with both the ductility and strength was determined. The determination of an ideal parameter set seen in Table 5 was selected for M300 maraging steel printed in a Renishaw AM400. The set of parameters was selected due to its ultimate tensile strength, elongation to failure, energy absorption, hardness, and surface roughness. Further work is needed to provide more information on the microstructure and the cause of the parameter sets performance. This work may include porosity measurements, microstructure analysis, and EBSD.

**Table 5:** Ideal set of process parameters for M300

Laser Power (W)	Scan Speed (mm/sec)	Spot Diameter (µm)	Hatch Distance (µm)	Layer Thickness (µm)	Exposure Time (µs)	Energy Density (J/mm <sup>3</sup> )
300	700	70	95	40	85.7	<b>112.78</b>

### Acknowledgments

The research described and the resulting data presented herein, unless otherwise noted, was funded under BAA 18-0099, GSL-3 "Ground Vehicles Mobility Research", Task 8 under Contract No. W912HZ-19-C-0036, managed by the Engineer Research and Development Center (ERDC). The work described in this presentation was conducted at the Center for Advanced Vehicular Systems. Permission was granted by ERDC to publish this information.

### References

- [1] B. Mooney and K. I. Kourousis, "A Review of Factors Affecting the Mechanical Properties of Maraging Steel 300 Fabricated via Laser Powder Bed Fusion," *Metals*, vol. 10, no. 9, p. 1273, 2020.
- [2] X. Mei, Y. Yan, H. Fu, X. Gao, S. Huang, and L. Qiao, "Effect of aging temperature on microstructure evolution and strengthening behavior of L-PBF 18Ni(300) maraging steel," *Additive Manufacturing*, vol. 58, p. 103071, Oct. 2022, doi: 10.1016/j.addma.2022.103071.
- [3] T. H. Becker and D. Dimitrov, "The achievable mechanical properties of SLM produced Maraging Steel 300 components," *Rapid Prototyping Journal*, vol. 22, no. 3, pp. 487–494, 2016.
- [4] Y. M. Arisoy, L. E. Criales, T. Özel, B. Lane, S. Moylan, and A. Donmez, "Influence of scan strategy and process parameters on microstructure and its optimization in additively manufactured nickel alloy 625 via laser powder bed fusion," *Int J Adv Manuf Technol*, vol. 90, no. 5–8, pp. 1393–1417, May 2017, doi: 10.1007/s00170-016-9429-z.
- [5] S. Dehgahi, R. Alaghmandfard, J. Tallon, A. Odeshi, and M. Mohammadi, "Microstructural evolution and high strain rate compressive behavior of as-built and heat-treated additively manufactured maraging steels," *Materials Science and Engineering: A*, vol. 815, p. 141183, May 2021, doi: 10.1016/j.msea.2021.141183.
- [6] J. Mutua, S. Nakata, T. Onda, and Z.-C. Chen, "Optimization of selective laser melting parameters and influence of post heat treatment on microstructure and mechanical properties of maraging steel," *Materials and Design*, vol. 139, pp. 486–497, 2018.
- [7] S. Yin *et al.*, "The influence of aging temperature and aging time on the mechanical and tribological properties of selective laser melted maraging 18Ni-300 steel," *Additive Manufacturing*, vol. 22, pp. 592–600, 2018.
- [8] I. Szachogłuchowicz, B. Fikus, K. Grzelak, J. Kluczyński, J. Torzewski, and J. Łuszczek, "Selective Laser Melted M300 Maraging Steel—Material Behaviour during Ballistic Testing," *Materials*, vol. 14, no. 10, p. 2681, May 2021, doi: 10.3390/ma14102681.
- [9] S. Shamsdini *et al.*, "Plastic deformation throughout strain-induced phase transformation in additively manufactured maraging steels," *Materials & Design*, vol. 198, p. 109289, Jan. 2021, doi: 10.1016/j.matdes.2020.109289.
- [10] C. Tan, K. Zhou, M. Kuang, W. Ma, and T. Kuang, "Microstructural characterization and properties of selective laser melted maraging steel with different build directions," *Science and Technology of Advanced Materials*, vol. 19, no. 1, pp. 746–758, 2018.
- [11] C. Tan, K. Zhou, W. Ma, P. Zhang, M. Liu, and T. Kuang, "Microstructural evolution, nanoprecipitation behavior and mechanical properties of selective laser melted high-performance grade 300 maraging steel," *Materials and Design*, vol. 134, pp. 23–24, 2017, doi: 10.1016/j.matdes.2017.08.026.
- [12] Y. Bai, Y. Yang, D. Wang, and M. Zhang, "Influence mechanism of parameters process and mechanical properties evolution mechanism of maraging steel 300 by selective laser melting," *Materials Science and Engineering: A*, vol. 703, pp. 116–123, Aug. 2017, doi: 10.1016/j.msea.2017.06.033.
- [13] M. Król, P. Snopiński, J. Hajnyš, M. Pagáč, and D. Łukowiec, "Selective Laser Melting of 18Ni-300 Maraging Steel," *Materials (Basel)*, vol. 13, no. 19, p. 4268, 2020, doi: 10.3390.

- [14] G. Stornelli, D. Gaggia, M. Rallini, and A. Di Schino, "Heat treatment effect on maraging steel manufactured by laser powder bed fusion technology: Microstructure and Mechanical Properties," *Acta Metallurgica Slovaca*, vol. 27, no. 3, pp. 122–126, 2021, doi: 10.36547.
- [15] D. D. Baere, M. Moshiri, L. Smolej, and J. H. Hattel, "Numerical investigation into laser-based powder bed fusion of cantilevers produced in 300-grade maraging steel," *Additive Manufacturing*, vol. 50, Feb. 2022, Accessed: Feb. 09, 2022. [Online]. Available: <https://www.sciencedirect.com/science/article/pii/S2214860421007077>
- [16] G. Casalino, S. L. Campanelli, N. Contuzzi, and A. D. Ludovico, "Experimental investigation and statistical optimisation of the selective laser melting process of a maraging steel," *Optical and Laser Technology*, vol. 65, pp. 151–158, 2015.
- [17] M. Król, P. Snopiński, and A. Czech, "The Phase Transition in selective laser-melted 18-Ni (300-grade) maraging steel," *Journal of Thermal Analysis and Calorimetry*, vol. 142, pp. 1011–1018, 2020, doi: 10.1007/s10973-020-09316-4.
- [18] T. Burkert and A. Fischer, "THE EFFECTS OF HEAT BALANCE ON THE VOID FORMATION WITHIN MARAGE 300 PROCESSED BY SELECTIVE LASER MELTING," p. 13.
- [19] E. Cyr, A. Lloyd, and M. Mohammadi, "Tension-compression asymmetry of additively manufactured Maraging steel," *Journal of Manufacturing Processes*, vol. 35, pp. 289–294, Oct. 2018, doi: 10.1016/j.jmapro.2018.08.015.
- [20] J. Suryawanshi, K. G. Prashanth, and U. Ramamurty, "Tensile, fracture, and fatigue crack growth properties of a 3D printed maraging steel through selective laser melting," *Journal of Alloys and Compounds*, vol. 725, pp. 355–364, Nov. 2017, doi: 10.1016/j.jallcom.2017.07.177.
- [21] R. Branco, J. D. Costa, J. A. M. Ferreira, C. Capela, F. V. Antunes, and W. Macek, "Multiaxial Fatigue behaviour of maraging steel produced by selective laser melting," *Materials and Design*, vol. 201, 2021, Accessed: Feb. 14, 2022. [Online]. Available: <https://reader.elsevier.com/reader/sd/pii/S0264127521000228?token=CCF818E03F0DD3D6F760ED3D9F86D0A4676580AC973999283DF2E142A600A4AE25005C81612596FBBB0EC3B995B5D45E&originRegion=us-east-1&originCreation=20220214212937>
- [22] K. Kempen, E. Yasa, L. Thijs, J.-P. Kruth, and J. Van Humbeeck, "Microstructure and mechanical properties of Selective Laser Melted 18Ni-300 steel," *Physics Procedia*, vol. 12, pp. 255–263, Jan. 2011, doi: 10.1016/j.phpro.2011.03.033.
- [23] R. Eisseler, D. Gutsche, C. Maucher, and H.-C. Möhring, "Inverse Determination of Johnson–Cook Parameters of Additively Produced Anisotropic Maraging Steel," *Materials*, vol. 15, no. 1, p. 26, Dec. 2021, doi: 10.3390/ma15010026.
- [24] M. Neuenfeldt, F. Zanger, and V. Schulze, "Influence of lpbfd process parameters on milling of a maraging tool steel," *MM Science Journal*, vol. 2021-November, pp. 5030–5037, 2021, doi: 10.17973/MMSJ.2021\_11\_2021148.
- [25] Y. Bai, C. Zhao, D. Wang, and H. Wang, "Evolution mechanism of surface morphology and internal hole defect of 18Ni300 maraging steel fabricated by selective laser melting," *Journal of Materials Processing Technology*, vol. 299, p. 117328, Jan. 2022, doi: 10.1016/j.jmatprotec.2021.117328.
- [26] J. Song *et al.*, "Effect of remelting processes on the microstructure and mechanical behaviours of 18Ni-300 maraging steel manufactured by selective laser melting," *Materials Characterization*, vol. 184, p. 111648, Feb. 2022, doi: 10.1016/j.matchar.2021.111648.
- [27] J. Vishwakarma, K. Chattopadhyay, and N. C. Santhi Srinivas, "Effect of build orientation on microstructure and tensile behaviour of selectively laser melted M300 maraging steel," *Materials Science and Engineering: A*, vol. 798, p. 140130, Nov. 2020, doi: 10.1016/j.msea.2020.140130.
- [28] "COMPARISON OF SELECTIVE LASER MELTING OF 18NI MARAGING STEEL BY PXL AND M2 CUSING | MM Science Journal," [www.mmscience.eu](http://www.mmscience.eu).

- <https://www.mmscience.eu/journal/issues/december-2016/articles/comparison-of-selective-laser-melting-of-18ni-maraging-steel-by-pxl-and-m2-cusing> (accessed Apr. 11, 2022).
- [29] S. Shamsdini, S. Shakerin, A. Hadadzadeh, B. S. Amirkhiz, and M. Mohammadi, "A trade-off between powder layer thickness and mechanical properties in additively manufactured maraging steels," *Materials Science and Engineering: A*, vol. 776, p. 139041, Mar. 2020, doi: 10.1016/j.msea.2020.139041.
- [30] R. Casati, J. Lemke, A. Tuissi, and M. Vedani, "Aging Behaviour and Mechanical Performance of 18-Ni 300 Steel Processed by Selective Laser Melting," *Metals*, vol. 6, no. 9, p. 218, Sep. 2016, doi: 10.3390/met6090218.
- [31] J. Song *et al.*, "Effect of heat treatment on microstructure and mechanical behaviours of 18Ni-300 maraging steel manufactured by selective laser melting," *Optics & Laser Technology*, vol. 120, p. 105725, Dec. 2019, doi: 10.1016/j.optlastec.2019.105725.
- [32] A. F. de Souza, K. S. Al-Rubaie, S. Marques, B. Zluhan, and E. C. Santos, "Effect of laser speed, layer thickness, and part position on the mechanical properties of maraging 300 parts manufactured by selective laser melting," *Materials Science and Engineering: A*, vol. 767, p. 138425, Nov. 2019, doi: 10.1016/j.msea.2019.138425.
- [33] W. Wu *et al.*, "Microstructure and mechanical properties of maraging 18Ni-300 steel obtained by powder bed based selective laser melting process," *Rapid Prototyping Journal*, vol. 26, no. 8, pp. 1379–1387, Jan. 2020, doi: 10.1108/RPJ-08-2018-0189.
- [34] C. Elangeswaran, K. Gurung, R. Koch, A. Cutolo, and B. Van Hooreweder, "Post-treatment selection for tailored fatigue performance of 18Ni300 maraging steel manufactured by laser powder bed fusion," *Fatigue & Fracture of Engineering Materials & Structures*, vol. 43, no. 10, pp. 2359–2375, 2020, doi: 10.1111/ffe.13304.
- [35] A. Oliveira, J. Diaz, A. D. Nizes, A. Jardini, E. Del Conte, and J. Avila D., "Investigation of Building Orientation and Aging on Strength–Stiffness Performance of Additively Manufactured Maraging Steel," *Journal of Materials Engineering and Performance*, vol. 30, Jan. 2021, doi: 10.1007/s11665-020-05414-4.
- [36] S. Shamsdini *et al.*, "A relationship between the build and texture orientation in tensile loading of the additively manufactured maraging steels," *Additive Manufacturing*, vol. 41, p. 101954, May 2021, doi: 10.1016/j.addma.2021.101954.
- [37] M. Costas *et al.*, "Ballistic impact resistance of additive manufactured high-strength maraging steel: An experimental study," *International Journal of Protective Structures*, vol. 12, no. 4, pp. 577–603, Dec. 2021, doi: 10.1177/20414196211035486.
- [38] "On the nature of the anisotropy of Maraging steel (1.2709) in additive manufacturing through powder bed laser-based fusion processing | Elsevier Enhanced Reader." <https://reader.elsevier.com/reader/sd/pii/S0264127521001611?token=42B5E92BA27356231CCD712BE0E614DC9FF566C4640972550DBC2651307916AFB56249BB5292DD0D39C7D9DB7E4A5109&originRegion=us-east-1&originCreation=20230209175617> (accessed Feb. 09, 2023).
- [39] J. Doh, N. Raju, N. Raghavan, D. W. Rosen, and S. Kim, "Bayesian inference-based decision of fatigue life model for metal additive manufacturing considering effects of build orientation and post-processing," *International Journal of Fatigue*, vol. 155, p. 106535, Feb. 2022, doi: 10.1016/j.ijfatigue.2021.106535.
- [40] M. J. Paul, Y. Muniandy, J. J. Kruzic, U. Ramamurty, and B. Gludovatz, "Effect of heat treatment on the strength and fracture resistance of a laser powder bed fusion-processed 18Ni-300 maraging steel," *Materials Science and Engineering: A*, vol. 844, p. 143167, Jun. 2022, doi: 10.1016/j.msea.2022.143167.
- [41] "Laser powder bed fusion of high-strength maraging steel with concurrently enhanced strength and ductility after heat treatments | Elsevier Enhanced Reader."

- <https://reader.elsevier.com/reader/sd/pii/S0921509322012011?token=4AB9150448585396A86294570B689FD2D3CD5F1F3A46C0834E4B9217C8162732B318C1BBD99B72AD34C1ED451956D658&originRegion=us-east-1&originCreation=20230221173300> (accessed Feb. 21, 2023).
- [42] “Plane-strain fracture toughness of thin additively manufactured maraging steel samples | Elsevier Enhanced Reader.”  
<https://reader.elsevier.com/reader/sd/pii/S2214860421006564?token=2ED93DFA38A3BE8CC9566849E2EF268D6E4423B9F6BE84791D125A916A9786B24E2925CA17BC712C569F1B63D6A415BB&originRegion=us-east-1&originCreation=20230221181212> (accessed Feb. 21, 2023).
- [43] Z. Zhao *et al.*, “Texture dependence on the mechanical properties of 18Ni300 maraging steel fabricated by laser powder bed fusion,” *Materials Characterization*, vol. 189, p. 111938, Jul. 2022, doi: 10.1016/j.matchar.2022.111938.
- [44] Z. Mao, X. Lu, H. Yang, X. Niu, L. Zhang, and X. Xie, “Processing optimization, microstructure, mechanical properties and nanoprecipitation behavior of 18Ni300 maraging steel in selective laser melting,” *Materials Science and Engineering: A*, vol. 830, p. 142334, Jan. 2022, doi: 10.1016/j.msea.2021.142334.
- [45] R. Kannan and P. Nandwana, “Texture evolution during processing and post-processing of maraging steel fabricated by laser powder bed fusion,” *Scientific Reports*, vol. 12, p. 6396, Apr. 2022, doi: 10.1038/s41598-022-09977-1.
- [46] K. Chadha, Y. Tian, P. Bocher, J. G. Spray, and C. Aranas, “Microstructure Evolution, Mechanical Properties and Deformation Behavior of an Additively Manufactured Maraging Steel,” *Materials*, vol. 13, no. 10, Art. no. 10, Jan. 2020, doi: 10.3390/ma13102380.
- [47] S. Raghavan *et al.*, “Effect of post-treatment on local mechanical properties of additively manufactured impellers made of maraging steel,” *Rapid Prototyping Journal*, vol. 29, no. 3, pp. 594–611, Jan. 2022, doi: 10.1108/RPJ-03-2022-0089.
- [48] G. Meneghetti, D. Rigon, D. Cozzi, W. Waldhauser, and M. Dabalà, “Influence of build orientation on static and axial fatigue properties of maraging steel specimens produced by additive manufacturing,” *Procedia Structural Integrity*, vol. 7, pp. 149–157, 2017, doi: 10.1016/j.prostr.2017.11.072.
- [49] V. Alfieri, V. Giannella, F. Caiazzo, and R. Sepe, “Influence of position and building orientation on the static properties of LPBF specimens in 17-4 PH stainless steel,” *Forces in Mechanics*, vol. 8, p. 100108, Aug. 2022, doi: 10.1016/j.finmec.2022.100108.
- [50] C. Additive, “PowderRange M300 | Carpenter Additive.”  
<https://www.carpenteradditive.com/metal-powders/powderrange-m300> (accessed Jun. 26, 2023).
- [51] “ASTM E8/E8M standard test methods for tension testing of metallic materials,” 2016. doi: 10.1520/E0008.
- [52] J. Vishwakarma, K. Chattopadhyay, and N. C. Santhi Srinivas, “Effect of build orientation on microstructure and tensile behaviour of selectively laser melted M300 maraging steel,” *Materials Science and Engineering: A*, vol. 798, p. 140130, Nov. 2020, doi: 10.1016/j.msea.2020.140130.
- [53] S. Shamsdini, S. Shakerin, A. Hadadzadeh, B. S. Amirkhiz, and M. Mohammadi, “A trade-off between powder layer thickness and mechanical properties in additively manufactured maraging steels,” *Materials Science and Engineering: A*, vol. 776, p. 139041, Mar. 2020, doi: 10.1016/j.msea.2020.139041.
- [54] M. Costas *et al.*, “Ballistic impact resistance of additive manufactured high-strength maraging steel: An experimental study,” *International Journal of Protective Structures*, vol. 12, no. 4, pp. 577–603, Dec. 2021, doi: 10.1177/20414196211035486.
- [55] X. Mei, Y. Yan, H. Fu, X. Gao, S. Huang, and L. Qiao, “Effect of aging temperature on microstructure evolution and strengthening behavior of L-PBF 18Ni(300) maraging steel,” *Additive Manufacturing*, vol. 58, p. 103071, Oct. 2022, doi: 10.1016/j.addma.2022.103071.